Supervised 2-phase Segmentation of Porous Media with Known Porosity

Ivan Georgiev, Stanislav Harizanov, and Yavor Vutov

Institute of Information and Communication Technologies,
Bulgarian Academy of Science, Sofia, Bulgaria

Abstract. Porous media segmentation is a nontrivial and often quite inaccurate process, due to the highly irregular structure of the segmentation phases and the huge interaction among them. In this paper we perform a 2-class segmentation of a gray-scale 3D image under the restriction that the number of voxels within the phases are a priori fixed. Two parallel algorithms, based on the graph 2-Laplacian model [1] are proposed, implemented, and numerically tested.

1 Introduction

Porous materials are of current interest within a wide range of applications, where their properties strongly depend on various measurements such as absolute porosity, average pore size, size and shape of individual pores. Therefore, accurate segmentation of a 3D reconstruction image of the corresponding specimen is crucial in practice. Due to the highly irregular structure of the segmentation phases and the presence of noise in the image, such a task is nontrivial and sometimes impossible, unless additional information on the data is provided. In particular, the volume (thus, the cardinality) of the solid phase can be determined from its density and weight.

We consider a 2-phase segmentation that satisfies an equality solid phase volume constraint. Graph 2-Laplacian is used for the mathematical model [1–4]. The derived constraint optimization problem is NP-hard [5]. Hence, we propose two different relaxations of the problem that can be efficiently solved. The paper is organized as follows. In Section 2, notation is fixed and the 2-Laplacian model is introduced. The two relaxed modifications of the original optimization problem, together with algorithms for solving them, are described in Section 3. In Section 4, three numerical examples are considered and the different algorithms are compared. Conclusions are drawn in Section 5.

2 Mathematical Formulation of the Problem

Let us first give some preliminary definitions and fix the notation. We consider 3D gray-scale images $\bar{u} : \Omega \to [0, \nu]$, where Ω is a discrete box domain of dimensions n_1, n_2, and n_3, respectively, while ν is the maximal intensity of the image. For a simpler matrix-vector notation, we assume the image to be

column-wise reshaped as a vector $\bar{u} \in [0,\nu]^{\mathbf{n}}$, with $\mathbf{n} = \mathrm{card}(\Omega) = n_1 n_2 n_3$. We keep the same notation $\bar{u}$ for the vectorized image and it will be clear from the context which representation we consider. We denote via $\mathbb{I}_{\mathbf{n}} := \{1,\dots,\mathbf{n}\}$ the voxel index set. The discrete segment membership vector $v \in \{0,1\}^{\mathbf{n}}$ is used for image segmentation and for every $i \in \mathbb{I}_{\mathbf{n}}$, it indicates to which class the i-th voxel belongs to ("air" if $v(i) = 0$ or "metal" if $v(i) = 1$). The index set is split into two disjoint subsets $\mathbb{I}_{\mathbf{n}} = L \cup U$ of labeled and unlabeled points, respectively. Without loss of generality (after re-numeration) we consider $L = \{1,\dots,2\ell\}$, $U = \{2\ell+1,\dots,\mathbf{n}\}$, and we split $v = (v_L, v_U)^T$. Furthermore, $L = L_0 \cup L_1$, where $L_0 := \{i \in L | v_L(i) = 0\} = \{1,\dots,\ell\}$, $L_1 := \{i \in L | v_L(i) = 1\} = \{\ell+1,\dots,2\ell\}$.

The indicator function ι_C of a nonempty set C is given by

$$\iota_C(x) = \begin{cases} 0 & \text{if } x \in C, \\ +\infty & \text{otherwise.} \end{cases}$$

Finally, we denote by e the ones vector $(1,\dots,1)^T$ of the appropriate dimension.

2.1 Graph 2-Laplacian Model

Starting with some labeled voxels ($L \neq \emptyset$) we want to segment the unlabeled ones, using their similarities/differences to the former and among themselves. Following [1], we do so via minimizing

$$F(v) := \langle \triangle v, v\rangle = \frac{1}{2}\sum_{i,j=1}^{\mathbf{n}} w_{i,j}\big(v(i)-v(j)\big)^2,$$

with respect to v_U, where $\triangle$ denotes the (graph) 2-Laplacian [6, 7]

$$(\triangle v)(i) = \sum_{j=1}^{\mathbf{n}} w_{i,j}\left(v(i)-v(j)\right).$$

The weights are chosen similar to [1]. Let $\mathcal{N}_i^{geo} = \{j : \|j-i\|_1 = 1\}$ be the 1-neighborhood of $i \in U$. Then, for $j \in \mathcal{N}_i^{geo}$ we take $w_{i,j}^{geo} = \frac{1}{6}$. Our feature function f is a weighted average of the intensities of the voxel i and its neighbors

$$f(i) = \frac{1}{12}\Big(6\bar{u}(i) + \sum_{j\in\mathcal{N}_i^{geo}} \bar{u}(j)\Big).$$

We use it as a similarity measure to compute the other two types of weights

$$w_{i,j}^{pho} := \begin{cases} a_i e^{-(f(i)-f(j))^2} & \text{if } j \in \mathcal{N}_i^{pho}, \\ 0 & \text{otherwise,} \end{cases} \qquad w_{i,j}^{lab} := \begin{cases} b_i e^{-(f(i)-f(j))^2} & \text{if } j \in L, \\ 0 & \text{otherwise.} \end{cases}$$

The constants a_i, b_i normalize the weights, so that they sum up to 1 within each group. $\mathcal{N}_i^{pho}$ consists of the 4 voxels j in the $5\times5\times5$ cube $\|i-j\|_\infty \le 2$ that minimize $|f(i)-f(j)|$. Finally, $W = \max\left\{\tilde{W}, \tilde{W}^T\right\}$, where

$$W^* = \frac{1}{1+\nu^{\mathrm{pho}}}W^{geo} + \frac{\nu^{\mathrm{pho}}}{1+\nu^{\mathrm{pho}}}W^{pho},\ \tilde{W} = \max\left\{\frac{\nu^{\mathrm{lab}}}{1+\nu^{\mathrm{lab}}}W^{lab}, \frac{1}{1+\nu^{\mathrm{lab}}}W^*\right\}.$$

W is non-negative, symmetric. The parameters $\nu^{\text{pho}}, \nu^{\text{lab}}$ are positive. Let

$$W := \begin{pmatrix} W_{LL} & W_{LU} \\ W_{UL} & W_{UU} \end{pmatrix}; \qquad D := \operatorname{diag}(d_i)_{i=1}^{\mathbf{n}}, \;\; d_i := \sum_{j=1}^{\mathbf{n}} w_{i,j}, \;\; \forall i \in \mathbb{I}_{\mathbf{n}}.$$

Note that $W_{UL} = W_{LU}$ due to symmetry and $F(v) = \frac{1}{2} v^T (D - W) v$. W_{UU} is sparse, and (almost) row-normalized via $d_i \approx 1, \;\forall i \in U$. Since $\nu^{\text{lab}} > 0$, $\sum_{j \in L} w_{i,j} > 0, \;\forall i \in U$, $D_{UU} - W_{UU}$ is strictly diagonally dominant with non-positive non-diagonal entries, thus an M-matrix, and the problem

$$\operatorname*{argmin}_{0 \le v \le 1} F(v) \quad \text{subject to} \quad v_L(i) = \begin{cases} 0, i \in L_0, \\ 1, i \in L_1, \end{cases} \tag{1}$$

admits a unique solution $\bar{v}$, given by (see [1, Theorem 3.2.] for details)

$$\underbrace{(D_{UU} - W_{UU})}_{Q} \bar{v}_U = \underbrace{W_{UL} v_L}_{q}. \tag{2}$$

Since $Q^{-1}, q \ge \mathbf{0}$, $\mathbf{0} \le \bar{v} \le \mathbf{1}$. To ensure $\bar{v} \in \{0,1\}^{\mathbf{n}}$, hard thresholding with respect to the middle value 0.5 is typically used.

Such segmentation methods work fine for well-separated, smooth phases, but their performance is unclear in the presence of big interaction. In (homogeneous) porous media, the "air" consists of multiple, non-structured, possibly not even connected pores of various size and shape, that "cut" through the material. Combined with the inevitable noise and blur the input image possesses, segmentation (2) is often poor and unreliable. In this paper, we assume that the input is a 3D reconstruction of a given specimen, which volume is a priori known. Thus, the number of the solid phase voxels N is given and can be used as a constraint in the mathematical model. We consider the following problem

$$\operatorname*{argmin}_{v \in \{0,1\}^{\mathbf{n}}} F(v) \quad \text{subject to} \quad v_L(i) = \begin{cases} 0, i \in L_0, \\ 1, i \in L_1; \end{cases} \quad \|v\|_0 = N. \tag{3}$$

The ℓ_0 pseudo-norm is non-convex and the problem (3) is NP-Hard [5]. In the binary case, $\|v\|_0 = \|v\|_1 = e^T v$, thus we rewrite the problem accordingly

$$\operatorname*{argmin}_{v \in \{0,1\}^{\mathbf{n}}} F(v) \quad \text{subject to} \quad v_L(i) = \begin{cases} 0, i \in L_0, \\ 1, i \in L_1; \end{cases} \quad e^T v = N, \tag{4}$$

and apply convex optimization techniques to this convex reformulation.

3 Convex Optimization Algorithms

We propose 2 different algorithms for dealing with (4) - one direct, and one iterative. Both algorithms does not solve (4) itself, but further modifications of the problem. The algorithms' results are compared on several different inputs.

3.1 Equality Constrained Quadratic Optimization

If we forget about $v \in \{0,1\}^{\mathbf{n}}$, denote by $N_1 := N - \ell$, and use the notation from (2), we derive the equality constrained quadratic optimization problem

$$\underset{v_U}{\operatorname{argmin}} \frac{1}{2} v_U^T Q v_U - q^T v_U \quad \text{subject to} \quad e^T v_U = N_1. \tag{5}$$

Thus, the minimizer $\bar{v}_U$ of (5) is the solution of

$$\begin{pmatrix} Q & e \\ e^T & 0 \end{pmatrix} \begin{pmatrix} \bar{v}_U \\ \lambda \end{pmatrix} = \begin{pmatrix} q \\ N_1 \end{pmatrix}, \tag{6}$$

where λ is Lagrange multiplier. If $s := -e^T Q^{-1} e$ is the Schur complement, then (6) can be rewritten as

$$\begin{pmatrix} Q & \\ e^T & s \end{pmatrix} \begin{pmatrix} I & Q^{-1}e \\ & 1 \end{pmatrix} \begin{pmatrix} \bar{v}_U \\ \lambda \end{pmatrix} = \begin{pmatrix} q \\ N_1 \end{pmatrix} \quad \Rightarrow \quad \left| \begin{array}{l} \lambda = (N_1 - e^T Q^{-1} q)/s, \\ \bar{v}_U = Q^{-1} q + \lambda Q^{-1} e. \end{array} \right.$$

The matrix Q is sparse and positive definite. We use conjugate gradient (CG) method [8] for solving the linear systems $Qx = q$ and $Qy = e$. For the segment membership vector we take $(v_L, \hat{v}_U)^T$, where the N_1 largest elements of $\bar{v}_U$ are set to 1 (in case of equality, randomness is applied), while the rest are set to 0.

Since $(Qe)(i) = \sum_{j \in L} w_{i,j} \approx \frac{\nu^{\text{lab}}}{1+\nu^{\text{lab}}}$ (the value may slightly differ only for close neighbors $i \in U$ of L), we have that $Q^{-1}e \approx \frac{1+\nu^{\text{lab}}}{\nu^{\text{lab}}} e$. Hence $\bar{v}_U$ is basically a shift of the solution of (1), and the segmentation based on (5) coincides with the N-segmentation of (2).

We also consider a slight generalization of (6)

$$\begin{pmatrix} Q - 2\mu I & e \\ e^T & 0 \end{pmatrix} \begin{pmatrix} \bar{v}_U \\ \lambda \end{pmatrix} = \begin{pmatrix} q \\ N_1 \end{pmatrix}, \tag{7}$$

that corresponds to the penalized version

$$\underset{v_U, \lambda}{\operatorname{argmin}} \frac{1}{2} v_U^T Q v_U - q^T v_U + \lambda(e^T v_U - N_1) - \mu(v_U^T v_U - N_1)$$

of the Lagrange formulation of (5). The penalizer $\mu > 0$ aims at sparsifying the solution $\bar{v}_U$, because $0 \le v_U \le 1$, together with $e^T v_U \le N_1$ and $v_U^T v_U \ge N_1$, guarantee $v \in \{0,1\}^{\mathbf{n}}$, $e^T v = N$. In our experiments, we take $\mu = \nu^{\text{pho}}/(3(1 + \nu^{\text{pho}})) = \frac{1}{3} \min_{i \in U} \sum_{j \in L} w_{i,j}$ to assure that $Q - 2\mu I$ remains an M-matrix and CG solver for (7) still converges (fast).

3.2 Fully Constrained Convex ℓ_2-norm Minimization

Let $\mathbf{n}_1 = \mathbf{n} - 2\ell$. As in (5), we start by projecting (4) onto U

$$\underset{v_U \in \{0,1\}^{\mathbf{n}_1}}{\operatorname{argmin}} \frac{1}{2} v_U^T Q v_U - q^T v_U \quad \text{subject to} \quad e^T v_U = N_1.$$

For segment membership vectors $v_U^2 = v_U$, and the problem is equivalent to

$$\underset{v_U \in \{0,1\}^{\mathbf{n}_1}}{\operatorname{argmin}} \left\langle \underbrace{(Q - 2\operatorname{diag}(q))}_{\bar{Q}} v_U, v_U \right\rangle \quad \text{subject to} \quad e^T v_U = N_1. \tag{8}$$

Here $\operatorname{diag}(q)$ is the diagonal matrix, generated by q. Since

$$q_i = \sum_{j \in L} w_{i,j} u_L(j) = \sum_{j \in L_1} w_{i,j} \quad \Longrightarrow \quad \bar{Q} = \bar{D}_{UU} - W_{UU}.$$
$$\bar{D}_{UU} = \operatorname{diag}(\bar{d}), \quad \bar{d}(i) = \sum_{j \in L} (-1)^{u_L(j)} w_{i,j} + \sum_{j \in U} w_{i,j}, \ \forall i \in U.$$

We consider the following constrained ℓ_2-norm optimization problem:

$$\underset{v_U \in \{0,1\}^{\mathbf{n}_1}}{\operatorname{argmin}} \ \|\bar{Q} v_U\|_2^2 \quad \text{subject to} \quad e^T v_U = N_1. \tag{9}$$

The relation between (8) and (9) is given by the Cauchy-Schwarz inequality.

$$\langle \bar{Q} v_U, v_U \rangle \le \|\bar{Q} v_U\|_2 \|v_U\|_2 = \sqrt{N_1}\ \|\bar{Q} v_U\|_2.$$

For the equality, we used that if $v_U \in \{0,1\}^{\mathbf{n}_1}$, $(v_U - e)^T v_U = 0$. Next, we relax both the constraints in (9) so that the problem becomes convex

$$\underset{0 \le v_U \le 1}{\operatorname{argmin}} \|\bar{Q} v_U\|_2^2 \quad \text{subject to} \quad e^T v_U \ge N_1. \tag{10}$$

If the halfspace $H := \{x \in \mathbb{R}^{\mathbf{n}_1} \mid e^T x \ge N_1\}$ does not contain any zeroes of $\bar{Q}$, the minimizer $\bar{v}_U$ lies on its border and satisfies $e^T \bar{v}_U = N_1$. Similar conclusion cannot be drawn for the box constraint, and once again we take the N_1 largest entries of $\bar{v}_U$ to be "metal", while the rest we set as "air".

Following [10], we rewrite (10) into its equivalent form

$$\underset{v_U \in \mathbb{R}^{\mathbf{n}_1}, x \in \mathbb{R}^{3\mathbf{n}_1}}{\operatorname{argmin}} \left\{ \langle 0, v_U \rangle + \iota_H(x_1) + \|x_2\|_2^2 + \iota_{[0,1]^{\mathbf{n}_1}}(x_3) \right\} \text{ s.t. } \begin{pmatrix} I \\ \bar{Q} \\ I \end{pmatrix} v_U = \begin{pmatrix} x_1 \\ x_2 \\ x_3 \end{pmatrix},$$

and apply the alternating direction methods of multipliers (ADMM)

Algorithm (ADMM): Initialization: $q_{1,2,3}^{(0)} = 0$, $x_{1,3}^{(0)} = e$, $x_2^{(0)} = \bar{Q}e$, $\gamma \in (0,1)$. For $k = 0, 1, \ldots$ repeat until a stopping criterion is reached

1. $v_U^{(k+1)} = (\bar{Q}^T \bar{Q} + 2I)^{-1} \left(\left(x_1^{(k)} - q_1^{(k)}\right) + \bar{Q}^T \left(x_2^{(k)} - q_2^{(k)}\right) + \left(x_3^{(k)} - q_3^{(k)}\right) \right)$
2. $x_1^{(k+1)} = \begin{cases} q_1^{(k)} + v_U^{(k+1)}, & \left(q_1^{(k)} + v_U^{(k+1)}\right) \in H, \\ q_1^{(k)} + v_U^{(k+1)} + \frac{N_1 - e^T (q_1^{(k)} + v_U^{(k+1)})}{\mathbf{n}_1^2} e, & \text{otherwise.} \end{cases}$
3. $x_2^{(k+1)} = \gamma \left(q_2^{(k)} + \bar{Q} v_U^{(k+1)}\right)$
4. $x_3^{(k+1)} = \min\left(1, \max\left(0, q_3^{(k)} + v_U^{(k+1)}\right)\right)$
5. $q_i^{(k+1)} = q_i^{(k)} + v_U^{(k+1)} - x_i^{(k+1)}$, $i = 1, 3$, $\qquad q_2^{(k+1)} = q_2^{(k)} + \bar{Q} v_U^{(k+1)} - x_2^{(k+1)}$.

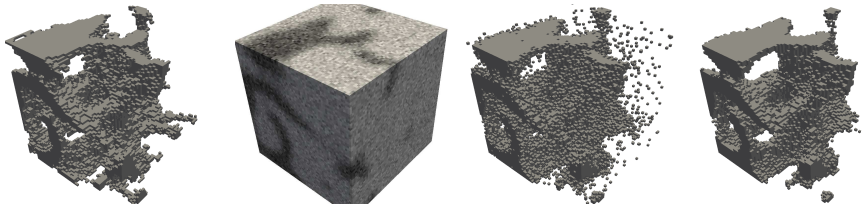

Fig. 1. From left to right: Segmented bone part (binary image), noisy and blurry input image $\bar{u}$, direct N-segmentation, segmentation based on (10).

Step 1 is solved (implicitly) via parallelized CG, since $\bar{Q}^T\bar{Q} + 2I$ is sparse and positive definite. Steps 3-5 are all componentwise, thus are parallelized, too. The complete splitting of the constraints, due to the introduction of $\langle 0, v_U \rangle$ in the cost function, leads to fast convergence rate of the algorithm.

4 Numerical Examples

In this section, we demonstrate by numerical examples the performance of our algorithms, implemented in C++. The code is parallelized using OpenMP [11]. The assembly of the matrix, matrix-vector, and vector operations is distributed among the available threads. We have tested artificially polluted bone part, based on [9]; a real 3D reconstruction of an Aluminum (AlSi10Mg) metal foam, obtained via industrial CT scan; and a binary image of a sphere inside a unit cube. We take $\ell = 3$, where L_0 (L_1) consists of the indices of the three voxels that minimize (maximize) f. When computing the weights, we use mirror boundary conditions. For the ADMM algorithm, we set $\gamma = 0.3$. In all the examples, the CG method converges fast, so no preconditioning is needed/used. Different segment vectors $v_{1,2} \in \{0,1\}^{\mathbf{n}}$ are compared via both their voxel difference $\|v_1 - v_2\|_1$ and their 2-sided Hausdorf distance, based on the 3D sup-norm $\|\cdot\|_\infty$.

The bone part image has size $64 \times 64 \times 64$. 50604 of its voxels are bone material (porosity 80.7%). The image was convoluted with a Gaussian kernel ($\sigma = 2$). Then, 10% white (Gaussian) noise was added to derive the input image $\bar{u}$ from Fig. 1. For the weight matrix W we used $\nu^{\text{pho}} = 10$, $\nu^{\text{lab}} = 0.1$.

As shown on Fig. 1 and in Table 1, simply taking the 50604 voxels of $\bar{u}$ highest intensity as the solid phase leads to poor segmentation, both visually and quantitatively. Our algorithms perfectly denoise $\bar{u}$, but are not able to completely

Table 1. Comparison among the original bone, its direct segmentation, and our algorithms. Above the diagonal: voxel difference, below: 2-sided Hausdorff distance.

hausd \ #voxels	original	direct	λ-QP (6)	$\mu\lambda$-QP (7)	ℓ_2-CP (10)
original	$*$	21 796	16 048	16 156	15 524
direct	25 547	$*$	10 476	10 412	11 346
λ-QP (6)	19 417	14 218	$*$	278	1 486
$\mu\lambda$-QP (7)	19 601	14 182	289	$*$	1 722
ℓ_2-CP (10)	18 857	15 140	1 509	1 764	$*$

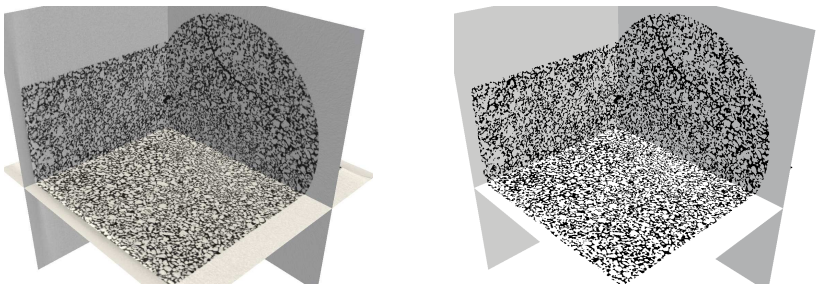

Fig. 2. 3 slices of the Aluminum foam reconstruction (left) and its segmentation via (10) (right).

Table 2. Comparison among different segmentations of the Aluminum metal foam. Above the diagonal: voxel difference, below: 2-sided Hausdorff distance.

hausd \ #voxels	direct	λ-QP (6)	$\mu\lambda$-QP (7)	ℓ_2-CP (10)
direct	$*$	2 789 328	2 850 756	2 659 200
λ-QP (6)	2 847 631	$*$	128 492	378 686
$\mu\lambda$-QP (7)	2 917 305	130 926	$*$	493 402
ℓ_2-CP (10)	2 702 613	384 633	503 522	$*$

overcome its blur. This results in thickening parts of the bone structure at the expense of loosing structure information elsewhere. Unlike the original image, the segmented one is not connected.

The AlSi10Mg foam reconstruction has size $680 \times 680 \times 680$ with sampling distance (voxel size) $0.0272mm$. The specimen has cylindrical shape with diam=$14.94mm$ and height=$16.55mm$ (see Fig. 2). Its weight is $2.7070g$ and $\rho(AlSi10Mg) = 2.6687g/cm^3$. Porosity is computed to be 83.97%, thus $N = 50405948$. Different segmentations are compared in Table 2. The ADMM algorithm converges fast (less than 70 iterations as shown on Fig. 3) as well as the CG solver within each step (less than 15 iterations per time).

With our last example (Fig. 4) we want to stress that our segmentation algorithms may still produce meaningful results when N differs from the real porosity. The input image is $64 \times 64 \times 64$ big, and the centered sphere takes 28% of its volume. We execute our algorithms with $N = 131072$ (half the volume). All the outputs are simply connected and visually resemble the original object.

5 Conclusions

Based on the 2-Lagrangian model in [1], we proposed two different relaxations for 2-phase image segmentation of a porous media of known porosity. The algorithms are implemented in a parallel way, allowing us to work with large 3D images of high resolution. The conducted numerical experiments showed significantly improved results, compared to non-supervised N-constrained segmentation. The outputs, based on (6), (7), and (10) are quite similar and there are no visible

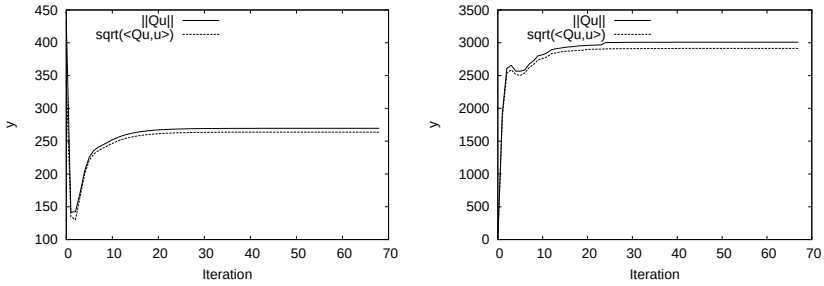

Fig. 3. Relation between (8) and (9): The graphs of $\sqrt{\langle \bar{Q} v_U^{(k)}, v_U^{(k)} \rangle}$ and $\|\bar{Q} v_U^{(k)}\|_2$ from the ADMM algorithm as functions of k. Left: Bone part. Right: Aluminum foam.

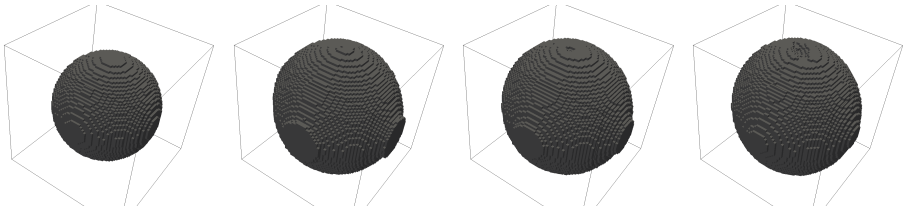

Fig. 4. From left to right: Original, segmented sphere inside a cube (volume = 28%). The output of (7), (6), (10), respectively, for volume = 50% of the cube's.

differences among them. Assuring connectivity of the solid phase is not achieved at this moment, and remains a task for future work.

Acknowledgements

The research is partly supported by the project AComIn "Advanced Computing for Innovation", grant 316087, funded by the FP7 Capacity Program.

References

1. Kang, S. H., Shafei, B., Steidl, G.: Supervised and transductive multi-class segmentation using p-Laplacians and RKHS methods. J. Visual Communication and Image Representation 25(5), 1136–1148 (2014)
2. Shi, J., Szalam, J.: Normalized cuts and image segmentation. IEEE Transactions on Pattern Analysis and Machine Intelligence 22(8), 888–905 (2000)
3. von Luxburg, U.: A tutorial on spectral clustering. Statistics and Computing 17(4), 395–416 (2007)
4. Law, N. Y., Lee, H. K., Ng, M. K., Yip, A. M.: A semisupervised segmentation model for collections of images. IEEE Trans. Image Processing 21(6), 2955–2968 (2012)
5. Natarajan, B. K.: Sparse approximate solutions to linear systems. SIAM J. Comput. 24(2), 227–234 (1995)

6. Amghibech, S.: Eigenvalues of the discrete p-Laplacian for graphs. Ars Combinatoria 67, 283–302 (2003)
7. Bühler, T., Hein, M.: Spectral clustering based on the graph p-Laplacian. In Proceedings of the 26th Ann. Intern. Conference on Machine Learning , 81–88 (2009)
8. Axelsson, A.: Iterative Solution Methods, Cambridge University Press (1994)
9. Beller, G., Burkhart, M., Felsenberg, D., Gowin, W., Hege, H.-C., Koller, B., Prohaska, S., Saparin, P., Thomsen, J.: Vertebral Body Data Set ESA29-99-L3. http://bone3d.zib.de/data/2005/ESA29-99-L3/
10. Teuber, T., Steidl, G., Chan, R. H.: Minimization and parameter estimation for seminorm regularization models with I-divergence constraints. Inverse Problems 29, 1–28 (2013)
11. Dagum, L., Menon, R.: OpenMP: an industry-standard API for shared-memory programming. IEEE Computational Science and Engineering 5(1), 46–55 (1998)